Program Digest, 2019 IEEE International Ultrasonics Symposium (IUS)
Glasgow, Scotland, October 6-9, 2019

A New Nonlinear Compounding Technique for Ultrasound B-mode Medical Imaging

Asraf Mohamed Moubark*, Luzhen Nie†, David M. J Cowell†, Sawal Hamid Md Ali* and Steven Freear†
*Center for Integrated Systems Engineering and Advanced Technologies, University Kebangsaan Malaysia, Selangor, Malaysia
†Ultrasound Group, School of Electronic and Electrical Engineering, University of Leeds, UK
E-mail: *asrafmohamed@ukm.edu.my and †S.Freear@leeds.ac.uk

***Abstract*—Compounding techniques have been used in ultrafast ultrasound imaging to improve image quality by reducing clutter noise, smoothing speckle variance and enhancing its spatial resolution at the cost of reducing frame rate. However, the reduction of clutter noise and side lobes inside the anechoic regions is minimal when combining conventional spatial compounding and delay-and-sum (DAS) beamforming. Despite the availability of advanced beamforming algorithms such as filtered-delay-multiply-and-sum (FDMAS), its prevalence is hindered by relatively high computational cost. In this study, a new nonlinear compounding technique known as filtered multiply and sum (FMAS) was proposed to improve the B-mode image quality without increasing the overall computational complexity. With three compunding angles, the lateral resolution for DAS-FMAS was improved by 36% and 19% compared to DAS and FDMAS. The proposed DAS-FMAS technique also provided improvements of 14.1 dB and 7.29 dB in contrast ratio than DAS and FDMAS.**

I. Introduction

Compounding techniques have been used in ultrafast ultrasound imaging to improve B-mode image quality by reducing clutter noise and smoothing speckle variance [1], [2]. However, the conventional compounding technique with coherent arithmetic averaging is not the most effective method since the reduction of clutter noise inside the anechoic regions is minimal. The reduction of side lobes is also ineffective. A number of steered plane waves are thus needed to achieve good spatial resolution which in return reduces the frame rate. The poor performance of conventional compounding is because that the side lobes occurring at diferent spatial locations are loosely correlated. This happens due to the different time delays used for each plane wave transmission. On the other hand, the main lobe position does not change and highly correlate between steered plane waves.

Recently, a new beamforming technique known as filtered delay multiply and sum (FDMAS) has been introduced in [3] to improve ultrasound image quality. However, the main drawback is the computational complexity (CC). Thus in this work, the FDMAS algorithm has been applied during compounding instead of the beamforming stage to reduce the CC and at the same time to improves the B-mode image qualities.

II. Materials and Methods

A. Filtered Multiply and Sum Beamforming

The proposed compounding technique takes place after beamforming echoes from multiple steered plane waves with DAS. Unlike the conventional compounding technique where all the steered plane waves are added and averaged after beamforming, the beamformed RF frames are multiplied and added to form the multiply and sum (MAS) frame. The MAS equation is given as follows

$$C_{\mathrm{MAS}} = \sum_{n=1}^{N-1} \sum_{k=n+1}^{N} \mathrm{sgn}\{V_n(t)V_k(t)\} \times \sqrt{|V_n(t)V_k(t)|}, \quad (1)$$

where $V(t)$ represents a set of aligned RF signals $V_i(t)$ ($i =$ 1 to 128) for each steered plane wave. The process is similar to the autocorrelation function. Instead of finding correlations between all channel RF signals to form an imaging line as in FDMAS, the proposed technique is faster due to the number of times of multiplication B involved in autocorrelation for FMAS is equal to the number of compounding angles N as given by :

$$B = \frac{N^2 - N}{2}, \quad (2)$$

The RF signals obtained from C_{MAS} need to be band pass filtered to produce filtered multiply-and-sum, C_{FMAS}. The reason is the same as that in FDMAS where two different frequency spectrums (DC and 2nd harmonics) are produced when two RF signals with the same frequency multiplied. Once filtered, the RF signals are Hilbert transformed for envelope detection and then log-compressed to form the B-mode image.

B. Compounding

Table I shows the main parameters used for the compounding process. The maximum steering angles sets within the sector angles, [θ°_{max}, θ°_{min}] $\pm$12. The frames rates calculated at 30 mm depth with speed of sound of 1540 m/s.

978-1-7281-4595-2/19/$31.00 ©2019 IEEE

TABLE I
COMPOUNDING PARAMETERS

Properties	Values						
No. of Compounding, N	1	3	5	7	9	13	25
Angle Increment, $\Delta\theta$	0	12	6	4	3	2	1
Frame Rates, $\|\|kHz\|\|$	26	9	5	4	3	2	1

C. Experiments

In order to validate the proposed methods, experiments were performed on wires, a tissue mimicking phantom (*040GSE, CIRS, Virginia, USA*) and *in-vivo*. The phantom with wires of 120 μm in diameter were imaged starting from 10 mm to 50 mm depth with a 10-mm spacing between every two wire targets. The hypo-echoic sections of the synthetic phantom were imaged at between 10 to 50 mm depth. *In-vivo* data were collected from the cross section of a right common carotid artery of a healthy volunteer. All measurements were performed with a 128-element linear array transducer (*L3-8/40EP, Prosonics Co. Ltd., Taiwan*). The transducer centre frequency was 4.79 MHz and it had a -6dB bandwidth of 57%. The transducer was excited with a multi-purpose imaging system (*UARPII, University of Leeds, UK*) [4]–[10]. The received signals from each channel were sampled at 80 MHz. The complete experimental parameters are given in Table II.

TABLE II
EXPERIMENTAL PARAMETERS

Properties	Values
Speed of Sound in Water/CIRS Phantom, m/s	1482/1540
Attenuation in Water/CIRS, dB/MHz/cm	0.002/0.5
Number of Elements	128
Transducer Centre Frequency, MHz	4.79
Transducer Bandwidth (-6 dB), %	57
Transducer Element Pitch, mm	0.3048
Sampling Frequency, Tx/Rx, MHz	160/80
Excitation	2-cycle Sinusoid

III. PERFORMANCE EVALUATION

The proposed compounding technique, FMAS was applied to the B-mode images beamformed with DAS. The results were compared with B-mode images beamformed with DAS and FDMAS and coherently compounded. To evaluate the final B-mode images formed with FMAS, DAS and FDMAS, several key performance indicators have been used. The main lobes resolution of the point target and its peak side lobe (PSL) were measured on wire phantom located at 30 mm depth with Full width half maximum (FWHM), -6 dB [11]. While the image contrast ratio (CR) and contrast-to-noise ratio (CNR) of a 15-mm deep hypoechoic cyst in the phantom was computed. Both CR and CNR equations are given by [12]

$$\text{CR(dB)} = 20\log_{10}\left(\frac{\mu_{cyst}}{\mu_{back}}\right), \tag{3}$$

$$\text{CNR(dB)} = 20\log_{10}\left(\frac{|\mu_{cyst} - \mu_{Back}|}{\sqrt{({\sigma_{cyst}}^2 + {\sigma_{Back}}^2)}}\right), \tag{4}$$

where μ_{cyst} and μ_{Back} are means of image intensities inside and outside of the cyst respectively, while ${\sigma_{cyst}}^2$ and ${\sigma_{Back}}^2$ are their variances. CR and CNR were calculated on the cyst by creating two different regions with the same dimensions. The first region was inside the cyst while the other region was located outside the cyst at the same depth. This was to ensure that depth-dependent attenuation caused by the depth does not affect the measurements.

IV. RESULTS

The B-mode images from experimental results for the wire target at 30 mm depth compounded with N=25 steering angles are presented in Fig. 1. The most significant improvement can be seen with DAS-FMAS as the side lobes along the lateral and axial directions have been reduced significantly. The lateral beam profiles for all three techniques are given in Fig. 2. Complete results for lateral resolution (LR) and PSL measured on the point targets are presented in Fig. 3.

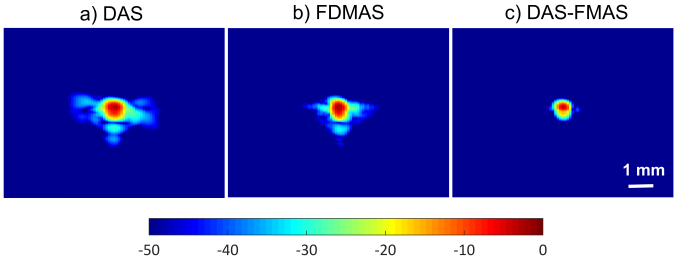

Fig. 1. B-mode images of the wire target beamformed using a) DAS, b) FDMAS and c) DAS-FMAS with 25 plane waves.

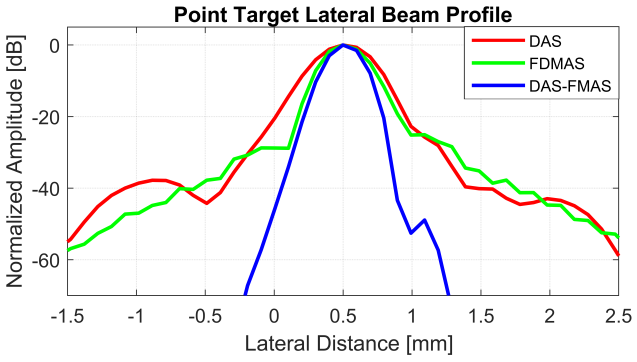

Fig. 2. Lateral beam profiles of the wire target at the depth of 30 mm when using beamforming techniques DAS, FDMAS and DAS-FMAS.

LR results at the -6 dB level for DAS, FDMAS and DAS-FMAS are given in Fig. 3(a). An improved LR is achieved with a lower number of compounding angles for all investigated techniques and DAS-FMAS produces the best results among

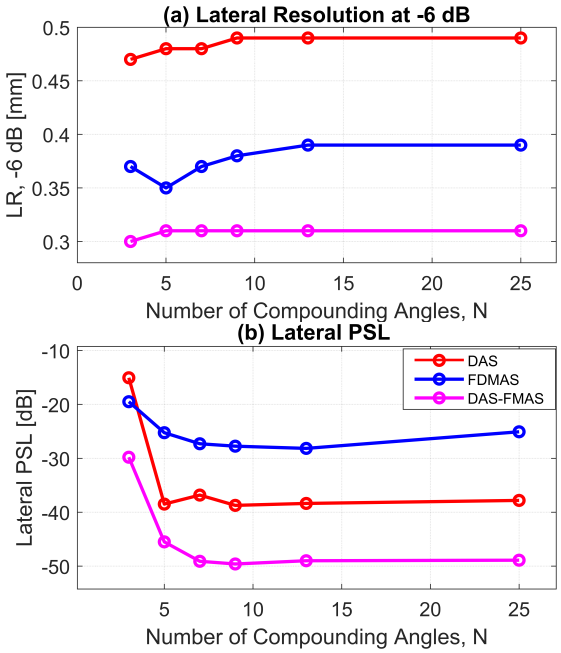

Fig. 3. LRs for DAS, FDMAS and DAS-FMAS at a) −6 dB level measured at 30 mm depth. The PSLs along the lateral direction are presented in (b).

them. At N=3, the LR for DAS-FMAS is improved by 36% and 19% compared to DAS and FDMAS. As the number of compounding angles increases to N=25, DAS-FMAS shows improvement by 37% and 20% compared to DAS and FDMAS. The LR for all techniques does not show any changes beyond N=13.

The PSLs in the lateral direction for DAS, FDMAS and DAS-FMAS are given in Fig. 3(b). All investigated techniques show improvement in reducing the PSL as the number of compounding angles increases from N=3 to N=25. DAS-FMAS gives the best results when compared to DAS and FMAS. At N=3, the PSL with DAS-FMAS has been reduced by 14.7 dB and 10.3 dB more than that using DAS and FDMAS, respectively. For N=25, the PSL has been reduced by 11.1 dB and 23 dB more with DAS-FMAS when compared to that using DAS and FDMAS.

At the depth of 15 mm, experimental results for the cyst of 3 mm in diameter are shown in Fig. 4, with N=25. The corresponding lateral beam profiles are shown in Fig. 5. The CRs for the cyst have been improved with FDMAS and DAS-FMAS compared to DAS. Qualitatively, it can be seen the reduction of clutter noise is more significant with DAS-FMAS compared to DAS and FDMAS. Complete CR results for the cyst are given in Fig. 6(a). The CRs for all techniques keep improving as the number of compounding angles increases. DAS-FMAS provides improvements of 14.1 dB and 7.29 dB than DAS and FDMAS with N=3. With N=25, the CR for DAS-FMAS is −49.8 dB which is the highest when compared to that using DAS (−26.1 dB) and FDMAS (−27.9 dB). No clutter noise is present inside the anechoic region with DAS-FMAS, as it has been attenuated below -60 dB, as shown in Fig. 5.

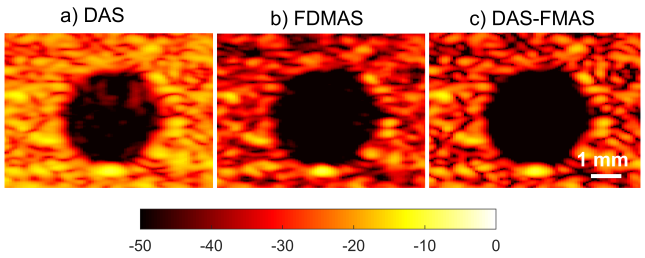

Fig. 4. B-mode images (N = 25) for a) DAS, b) FDMAS and c) DAS-FMAS.

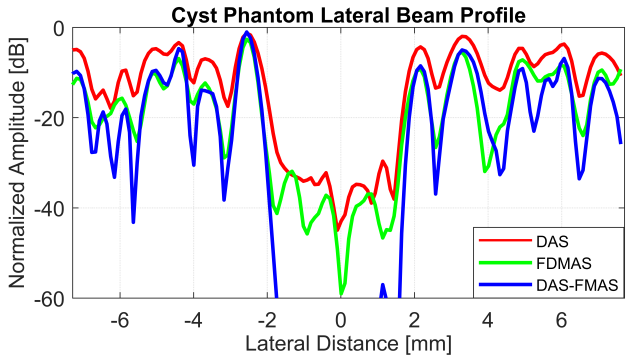

Fig. 5. Beam profiles for DAS, FDMAS and DAS-FMAS along the lateral direction at the 15 mm depth for the cyst of 3 mm in diameter.

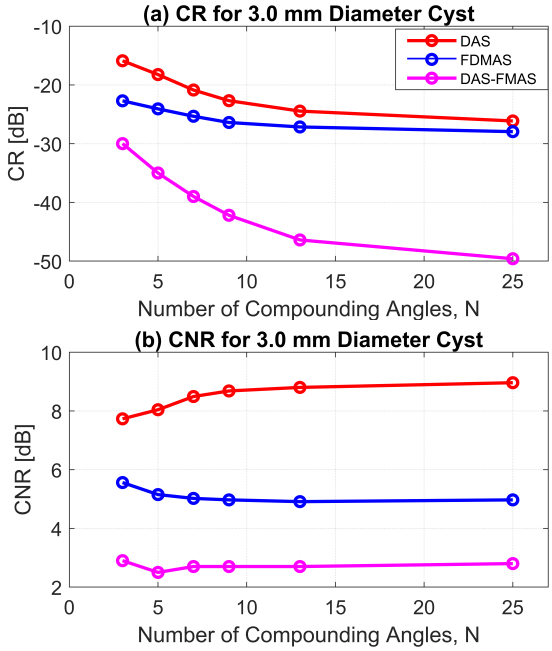

Fig. 6. a) CR and (b) CNRs using DAS, FDMAS and DAS-FMAS for the 3.0-mm cyst located at the depth of 15 mm.

The B-mode images for *in-vivo* measurements obtained using DAS, FDMAS and DAS-FMAS are presented in Fig. 7. Clutter noise reduction with FDMAS and DAS-FMAS

can be seen on the B-mode images starting from N=3. As the number of compounding angles increases to N=25, the common carotid artery and the near field regions are free of clutter noise with DAS-FMAS. With FDMAS, the side lobes in the lateral direction are still visible in the common carotid artery. Whereas with DAS clutter noise is still dominating most of the image.

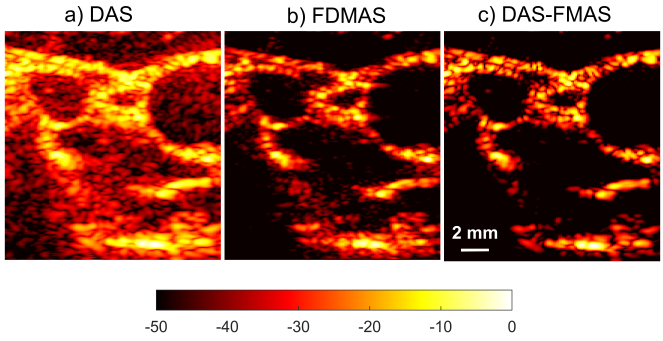

Fig. 7. B-mode images of a right side common carotid artery, N=25 formed with (a) DAS, (b) FDMAS and (c) DAS-FMAS.

The computational costs with DAS, FDMAS and DAS-FMAS for imaging wire target are given in Fig. 8. The computer operating system used to calculate the processing time is Windows 7 enterprise 64-bit. The computer specification is as follows: CPU (CORE i5-4460, Intel Corporation Co., Ltd., Santa Clara, CA, USA), 3.20-GHz clock speed, 4 cores and 16-GB DDR3 RAM. Thelateral beamforming step for DAS and FDMAS was set to $\lambda/3$=0.1 mm and for the axial direction it was c*T_s/2=9.625 μm. The width and depth of the imaging field are 60 mm and 39 mm. It can be seen that the computational time for DAS with conventional compounding is almost the same with that using DAS-FMAS. There is no significant difference between the processing time using DAS and DAS-FMAS. Whereas for FDMAS the computational time is 7 times longer than that with DAS and DAS-FMAS for N=25.

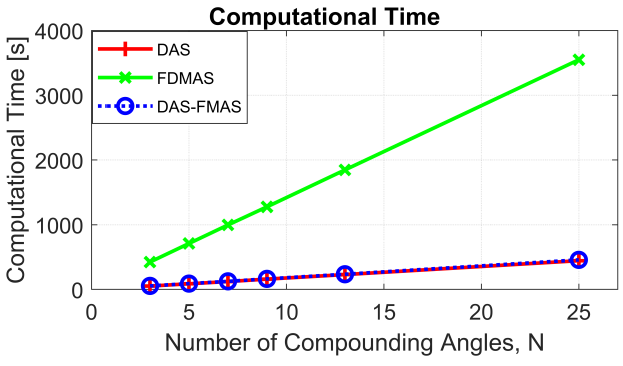

Fig. 8. Computational time measured for DAS, FDMAS and DAS-FMAS with different numbers of steering angles.

V. Conclusion

The proposed compounding technique FMAS is able to improve the B-mode image spatial resolution and CR compared to DAS and FDMAS. The CC of FDMAS is significantly higher than DAS and lower than other adaptive beamforming techniques such as minimum variance. However, keeping lowering the CC in FDMAS will be beneficial for real-time imaging and reducing the processing power. Thus, instead of applying FDMAS during beamforming, implementing FDMAS during compounding will not only reduce the CC, but also improve the overall B-mode image quality.

Acknowledgment

Part of this work was financially supported by Ministry of Higher education, Malaysia (Grant No. FRGS/1/2019/TK04/UKM/03/4). Funders were not involved in the conduct of the research.

References

[1] G. Montaldo, M. Tanter, J. Bercoff, N. Benech, and M. Fink, "Coherent plane-wave compounding for very high frame rate ultrasonography and transient elastography," *IEEE Transactions on Ultrasonics, Ferroelectrics, and Frequency Control*, vol. 56, no. 3, pp. 489–506, 2009.

[2] M. Toulemonde, O. Basset, P. Tortoli, and C. Cachard, "Thomson's multitaper approach combined with coherent plane-wave compounding to reduce speckle in ultrasound imaging," *Ultrasonics*, vol. 56, pp. 390–398, 2015.

[3] G. Matrone, A. Ramalli, A. S. Savoia, P. Tortoli, and G. Magenes, "High frame-rate, high resolution ultrasound imaging with multi-line transmission and filtered-delay multiply and sum beamforming," *IEEE Transactions on Medical Imaging*, vol. 36, no. 2, pp. 478–486, Feb 2017.

[4] P. R. Smith, D. M. J. Cowell, and S. Freear, "Width-modulated square-wave pulses for ultrasound applications," *IEEE Transactions on Ultrasonics, Ferroelectrics, and Frequency Control*, vol. 60, no. 11, pp. 2244–2256, November 2013.

[5] P. R. Smith, D. M. Cowell, and S. Freear, "Width-modulated square-wave pulses for ultrasound applications," *IEEE transactions on ultrasonics, ferroelectrics, and frequency control*, vol. 60, no. 11, pp. 2244–2256, 2013.

[6] P. R. Smith, D. M. Cowell, B. Raiton, C. V. Ky, and S. Freear, "Ultrasound array transmitter architecture with high timing resolution using embedded phase-locked loops," *IEEE transactions on ultrasonics, ferroelectrics, and frequency control*, vol. 59, no. 1, pp. 40–49, 2012.

[7] D. Cowell and S. Freear, "Quinary excitation method for pulse compression ultrasound measurements," *Ultrasonics*, vol. 48, no. 2, pp. 98–108, 2008.

[8] D. M. Cowell, P. R. Smith, and S. Freear, "Phase-inversion-based selective harmonic elimination (pi-she) in multi-level switched-mode tone- and frequency-modulated excitation," *IEEE transactions on ultrasonics, ferroelectrics, and frequency control*, vol. 60, no. 6, pp. 1084–1097, 2013.

[9] D. M. Cowell and S. Freear, "Separation of overlapping linear frequency modulated (lfm) signals using the fractional fourier transform," *IEEE Transactions on Ultrasonics, Ferroelectrics, and Frequency Control*, vol. 57, no. 10, pp. 2324–2333, 2010.

[10] S. Freear, D. M. J. Cowell, and P. R. Smith, "Ultrasound generation," Dec. 3 2015, uS Patent App. 14/653,781.

[11] S. Harput, J. McLaughlan, D. M. J. Cowell, and S. Freear, "New performance metrics for ultrasound pulse compression systems," in *2014 IEEE International Ultrasonics Symposium*, Sept 2014, pp. 440–443.

[12] A. M. Moubark, Z. Alomari, S. Harput, D. M. J. Cowell, and S. Freear, "Enhancement of contrast and resolution of b-mode plane wave imaging (pwi) with non-linear filtered delay multiply and sum (fdmas) beamforming," in *2016 IEEE International Ultrasonics Symposium (IUS)*, Sept 2016, pp. 1–4.